ilmedia

TECHNISCHE UNIVERSITÄT
ILMENAU

Merker, Lukas; Will, Christoph; Steigenberger, Joachim; Behn, Carsten:

Object shape recognition and reconstruction using pivoted tactile sensors

Research Article

Object Shape Recognition and Reconstruction Using Pivoted Tactile Sensors

L. Merker [iD],[1] **C. Will,**[1] **J. Steigenberger,**[2] **and C. Behn** [iD][3]

[1]*Technical Mechanics Group, Technische Universität Ilmenau, Max-Planck-Ring 12, 98693 Ilmenau, Germany*
[2]*Institute of Mathematics, Technische Universität Ilmenau, Weimarer Straße 25, 98693 Ilmenau, Germany*
[3]*Department of Engineering and Natural Sciences, Merseburg University of Applied Sciences,*
 Eberhard-Leibnitz-Str. 2, 06217 Merseburg, Germany

Correspondence should be addressed to L. Merker; lukas.merker@tu-ilmenau.de and C. Behn; carsten.behn@tu-ilmenau.de

Many mammals use some special tactile hairs, the so-called mystacial macrovibrissae, to acquire information about their environment. In doing so, rats and mice, e.g., are able to detect object distances, shapes, and surface textures. Inspired by the biological paradigm, we present a mechanical model for object contour scanning and shape reconstruction, considering a single vibrissa as a cylindrically shaped Euler-Bernoulli-bending rod, which is pivoted by a bearing. In doing so, we adapt our model for a rotational scanning movement, which is in contrast to many previous modeling approaches. Describing a single rotational quasi-static sweep of the vibrissa along a strict convex contour function using nonlinear Euler-Bernoulli theory, we end up in a boundary-value problem with some unknown parameters. In a first step, we use shooting methods in an algorithm to repeatedly solve this boundary-value problem (changing the vibrissa base angle) and generate the support reactions during a sweep along an object contour. Afterwards, we use these support reactions to reconstruct the object contour solving an initial-value problem. Finally, we extend the scanning process adding a second sweep of the vibrissa in opposite direction in order to enlarge the reconstructable area of the profile.

1. Introduction

Tactile sensors are frequently used in uncertain (changing, dark, noisy) environments, where optical sensors reach their capability. In many areas of application, e.g., in mobile robotics, tactile sensors are designed from simple passive impact sensors all the way through to complex, integrated systems, giving more detailed contact information. Since a large number of technical implementations are inspired by nature, it is well worth taking a brief view to the biological paradigm.

Rodents like rats and mice use their mystacial macrovibrissae (prominent tactile hairs in their snout region) for exploring the environment. The facial vibrissae array (mystacial pad) consists of a variety of vibrissal systems, each consisting of a hair shaft, which is embedded in its own support—the so-called follicle-sinus complex (FSC). A vibrissa itself does not consist of any sensory components but transmits mechanical stimuli to the FSC, where the actual perception of

stimuli happens. Therefore, the FSC is equipped with a variety of mechanoreceptors converting tactile information into neural impulses for the central nervous system [1]. In addition, the FSC is surrounded by an extrinsic and intrinsic musculature, which enables rats and mice to use their vibrissae in two very special modes [2, 3]:

(i) a passive mode without activating the musculature, in which each vibrissa is deformed only due to external forces (e.g., wind or mechanical contacts, when the animal is passing an object)

(ii) an active exploration mode whereby the vibrissae can be swept back and forth along obstacles rotationally by alternating contraction of the intrinsic and extrinsic musculature.

The active exploration mode, also known as active "whisking" is primary used to detect object surface or shape information.

Previous technical solutions of biological inspired tactile sensors are of different complexity depending on the purpose of use. In the most trivial case, an artificial vibrissa is used as a passive contact detector providing a binary contact signal. In mobile robotics, simple systems like these are already usable for obstacle collision avoidance [4] or autonomous wall following robot movements [5]. Other tactile sensor systems provide even more detailed information like object distances, shapes, or surface textures.

Works focussing the contact sensing problem from a dynamic point of view are, for instance, [6–9]. The authors in [8, 9] focus on a dynamic active antenna sensing in analyzing the natural resonance frequencies to determine the distance to an object. The dynamic approach therein is in contrast to our work, since we focus on a quasi-static movement of the support deflection angle. Further on, the boundary conditions in [8, 9] represent a bearing as a contact of the rod with an object. This contradicts the real behavior. The authors should analyze a one-sided contact restriction, but not a simple support as a contact scenario. Moreover, it seems that there are some problems in identifying the contact point in observing only the behavior of the eigenvalues and natural frequencies. Having a glance to the natural frequency plot [9, Figure 5], one can observe nearly two possibilities of a contact close to $z = 0.628$ and $z = 1.0$. The authors in [7] resolve this problem in designing the sensing rod within an elastic foundation. While [8, 9] are limited to the detection of the obstacle distance in determining only one contact point, this paper furthermore presents a procedure of reconstructing a whole part of an object contour.

Scanning an object, different information at the support of the rod (e.g., reaction forces and moments) can be used to determine the contact position. The object reconstruction process is considered in [10–12] as well, neglecting all dynamic aspects, but only using linear bending theory, which is not suitable for the large deflections of the vibrissa, which actually occur in reality. Due to the limitation to small deflections, the scanning process is frequently realized by rotating the artificial vibrissa by small pushing angles against an object [12] and not by an actual scanning sweep including large deflections, as it can be observed in animal's kingdom. A big disadvantage of using only small pushing angles is the need of changing the support position in order to scan a larger part of the object contour. In contrast, this problem does not occur within the present paper. It is shown that, considering large bending deflections described by nonlinear theory, it is possible to reconstruct a larger part of any object contour even without changing the support position.

Even though some previous publications consider large deflections as well, the scanning process is frequently realized by a translational scanning movement [13–17]. There, the authors describe a quasi-static translational sweep of a single rod, which is one-sided clamped, along a strict convex profile. Firstly, the scanning process is treated analytically as far as possible in order to generate the unknown support reactions, when the rod is swept along a profile contour. This analytical approach is in contrast to just performing experiments and measurements. Afterwards, the support reactions are used to determine a sequence of contact points, which approximate

the object contour. However, compared with the biological paradigm, the considered models (translational movement) rather represent the passive mode of an operating vibrissa. The animal's ability to actively rotate its vibrissae back and forth is not taken into account there.

Other works consider a rotary scanning movement, but the contact sensing problem or reconstruction process is always based on measurements only. For example, in [18, 19], a single artificial vibrissa is swept along an object rotationally by a DC-motor, whereby the support reactions are measured in a load cell. At different points in time, the elastic line of the vibrissa is determined by numerically integrating the deformation equations. A variety of deformation states finally makes the object contour apparent. Nevertheless, there is no mechanical model allowing for a theoretical generation of the support reactions. For that reason, it is not possible to carry out parameter studies with regard to different geometric properties of the vibrissa without the need of performing a large number of experiments.

Although some publications take various morphological characteristics like the elasticity of the FSC [17] or the tapered and precurved geometry of a vibrissa into account [20–23], there is no mechanical model for generating the support reactions during a rotary scanning sweep as well.

Within the present paper we limit ourselves to the main functionality of a rotary scanning movement and the biological requirement, that only the support of the rod can be used for detecting mechanical stimuli. Thus, we focus on a kind of an active vibrissa movement behavior starting with a general modeling of a rotary sweep along a strict convex object contour using a single technical vibrissa. A theoretical treatment of the scanning process will provide a basis for an algorithm, which is used for

(i) solving a boundary-value problem to generate the support reactions during a rotary scanning sweep,

(ii) solving an initial-value problem to reconstruct the object contour only using the generated observables.

The algorithm allows the generation of the support reactions needed for the reconstruction including large bending deflections, which is new in literature. Afterwards, numerical simulations are performed to demonstrate the functional capability of the algorithm. In addition, the scanning process is extended in a further step by a second sweep in opposite direction in order to enlarge the scanning range. The governed results extend and complement the ones from [13–17, 24].

2. General Modeling of a Rotational Sweep

Figure 1 shows the presented model, which is based on the following assumptions:

(i) **Vibrissa:**

(a) The vibrissa is modeled as a cylindrically shaped Euler-Bernoulli bending rod of length L. It is assumed to have a constant second moment of
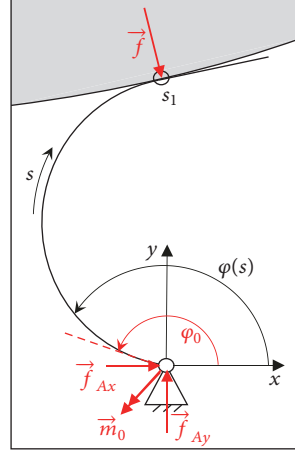
FIGURE 1: Mechanical model of a rotatable vibrissa sweeping along a strict convex object.

area I_z and a constant Young's modulus E—describing a linear elastic material behavior of the rod.

(b) The rod undergoes large deflections which are described using nonlinear Euler-Bernoulli theory.

(ii) **Support and drive:**

(a) The rod is pivoted rotationally by a bearing.

(b) Its base angle φ_0 (drive angle) is increased incrementally in order to generate a rotational planar vibrissa movement in a mathematical positive sense with respect to the z-axis. Therefore, the required holding moment $\vec{m}_0$ is calculated.

(iii) **Object and contact:**

(a) The object is modeled as a rigid body with a **strict convex** contour function $g : x \mapsto g(x)$.

(b) Due to the strict convexity, the contour function $g : x \mapsto g(x)$ can be parameterized by means of its slope angle $\alpha \mapsto (\xi(\alpha), \eta(\alpha)), \alpha \in (-\pi/2, \pi/2)$.

(c) During scanning for each preset drive angle φ_0 some point s_1 of the vibrissa undergoes a contact force $\vec{f}$ due to the contact with a specific unknown profile point, which is determined by a unique α.

(d) The strict convex object shape ensures that for each deformation state there is only **one contact point** with the object.

(e) The contact is considered as an **ideal contact**, so (ignoring friction effects) the contact force is always perpendicular to the profile tangent.

Using the nonlinear Euler-Bernoulli bending theory, the curvature $\kappa(s)$ of the deflected bending rod can be given in dependence on the natural coordinate arc length s [25]:

$$\kappa(s) = \frac{m_{bz}(s)}{EI_z} \tag{1}$$

where $m_{bz}(s)$ denotes the bending moment with respect to the z-axis. If the bending rod axis is parameterized by means of its slope angle $\varphi(s)$, we have

$$\begin{aligned} \frac{dx(s)}{ds} &= \cos(\varphi(s)), \\ \frac{dy(s)}{ds} &= \sin(\varphi(s)), \\ \frac{d\varphi(s)}{ds} &= \kappa(s). \end{aligned} \tag{2}$$

Remark 1. For a dimensionless representation we introduce some dimensionless parameters. At first, consider the definition of the arc length:

$$s := s^* \cdot \widetilde{s} \tag{3}$$

where s is the quantity in dimensions, s^* is the unit of s, and $\widetilde{s}$ is the dimensionless parameter (a number). Let us choose

$$s^* = L \tag{4}$$

which implies

$$\widetilde{s} = \frac{s}{s^*} = \frac{s}{L} \tag{5}$$

with $[\widetilde{s}] = 1$, $[s] = [s^*] = [L]$ and $s \in [0, L]$, $\widetilde{s} \in [0, 1]$.

In a similar way we proceed in considering the x-coordinate

$$\begin{aligned} x(s) &= x^* \cdot \widetilde{x}(\widetilde{s}) \\ \implies \frac{dx(s)}{ds} &= \frac{d(x^* \cdot \widetilde{x}(\widetilde{s}))}{ds} = \frac{d(x^* \cdot \widetilde{x}(\widetilde{s}))}{d\widetilde{s}} \frac{d\widetilde{s}}{ds} \\ &= x^* \cdot \frac{d(\widetilde{x}(\widetilde{s}))}{d\widetilde{s}} \frac{d\widetilde{s}}{ds} = x^* \cdot \frac{1}{L} \cdot \frac{d\widetilde{x}(\widetilde{s})}{d\widetilde{s}}. \end{aligned} \tag{6}$$

Obviously, the unit of x (meaning x^*) has to be L, and this implies $x = L \cdot \tilde{x}$ and $y = L \cdot \tilde{y}$. Transforming the differential equation of the slope angle φ, we have

$$\varphi(s) = \varphi^* \cdot \tilde{\varphi}(\tilde{s}) \tag{7}$$

with

$$\frac{d\varphi(s)}{ds} = \frac{d\left(\varphi^* \cdot \tilde{\varphi}(\tilde{s})\right)}{ds} = \varphi^* \cdot \frac{d\left(\tilde{\varphi}(\tilde{s})\right)}{d\tilde{s}} \frac{d\tilde{s}}{ds}$$
$$= \varphi^* \cdot \frac{1}{L} \cdot \frac{d\tilde{\varphi}(\tilde{s})}{d\tilde{s}} \tag{8}$$

Inserting into the differential equation (1), we get:

$$\frac{d\varphi(s)}{ds} = \kappa(s) = \frac{m_{bz}(s)}{EI_z}$$
$$\implies \varphi^* \cdot \frac{1}{L} \cdot \frac{d\tilde{\varphi}(\tilde{s})}{d\tilde{s}} = \frac{m_{bz}^* \cdot \tilde{m}_{bz}(\tilde{s})}{EI_z} \tag{9}$$
$$\iff \frac{d\tilde{\varphi}(\tilde{s})}{d\tilde{s}} = \frac{L}{EI_z} \cdot \frac{1}{\varphi^*} \cdot m_{bz}^* \cdot \tilde{m}_{bz}(\tilde{s}).$$

In order to cancel all dimensions, we choose

$$\varphi^* = 1,$$
$$m_{bz}^* = \frac{EI_z}{L}. \tag{10}$$

Summing up, we get the following dimensions:

$$[length] := L;$$
$$[moment] := EI_z L^{-1}; \tag{11}$$
$$[force] := EI_z L^{-2}.$$

Remark 2. As from now, we only use dimensionless quantities and drop all tildes ($\sim$) for reasons of clarity.

The constitutive law (1) then writes as

$$\kappa(s) = m_{bz}(s). \tag{12}$$

According to our assumptions the contact force $\vec{f}$ is perpendicular to the profile tangent:

$$\vec{f} = f\left(\sin(\alpha)\vec{e}_x - \cos(\alpha)\vec{e}_y\right) \tag{13}$$

Using (13) we can express the bending moment:

$$m_{bz}(s) = \begin{cases} f\left((y(s) - \eta(\alpha))\sin(\alpha) + (x(s) - \xi(\alpha))\cos(\alpha)\right) & s \in [0, s_1) \\ 0 & s \in (s_1, 1] \end{cases} \tag{14}$$

with $x(s_1) = \xi(\alpha)$ and $y(s_1) = \eta(\alpha)$.

Together with (2), (12), and (14) we end up in a system of ordinary differential equations of the first order, which describes the elastic line of any deflected bending rod (under the given assumptions):

(a) $x'(s) = \cos(\varphi(s))$

(b) $y'(s) = \sin(\varphi(s))$

(c) $\varphi'(s)$ $\tag{15}$

$= f\left((y(s) - \eta(\alpha))\sin(\alpha) + (x(s) - \xi(\alpha))\cos(\alpha)\right).$

We introduce a differential equation for the curvature by differentiating (15)(c) using (15)(a) and (15)(b) in order to get rid of the constants:

$$\frac{d\kappa(s)}{ds} = f\left(\frac{dy(s)}{ds}\sin(\alpha) + \frac{dx(s)}{ds}\cos(\alpha)\right)$$
$$= f\left(\sin(\varphi(s))\sin(\alpha) + \cos(\varphi(s))\cos(\alpha)\right) \tag{16}$$
$$= f\cos(\varphi(s) - \alpha).$$

The ODE system (15) describing the elastic line and then writes as

(a) $x'(s) = \cos(\varphi(s))$

(b) $y'(s) = \sin(\varphi(s))$

(c) $\varphi'(s) = \kappa(s)$ $\tag{17}$

(d) $\kappa'(s) = f\cos(\varphi(s) - \alpha).$

For further investigations we have to divide the scanning process into the following steps:

(i) **Step 1, Generating the Observables (Support Reactions).** In this step, we assume an object contour $\xi(\alpha), \eta(\alpha)$ to be given and determine the support reactions during scanning. In doing so we provide the observables that we will need for the reconstruction process in Step 2 and we obtain a better understanding about the influence of some important parameters on the scanning process.

(ii) **Step 2, Reconstructing the Object Contour.** In this step, we use the observables which are known from Step 1 (or might be known by measurement) in

order to determine a sequence of contact points between the bending rod and the object which finally approximates the object contour.

Remark 3. In an experimental setup, Step 1 could be replaced by measuring the observables in a load cell.

3. Step 1, Generating the Observables

To formulate the boundary conditions, a distinction between tip and tangential contact (Phase A and Phase B, respectively) of the rod with the object is made (see Figure 2):

(i) **Phase A, contact at the tip:** contact at $s_1 = 1$ with an unknown contact angle $\varphi(1) > \alpha$.

(ii) **Phase B, tangential contact:** contact at an unknown position $s_1 \in (0, 1)$ with contact angle $\varphi(s_1) = \alpha$.

For Step 1 we assume the following parameters to be known:

$$\boxed{x_0, y_0, \alpha, \xi(\alpha), \eta(\alpha)}. \tag{18}$$

The unknown parameters in Phases A and B can be determined using shooting methods to solve the following BVPs:

Phase A ($s \in (0, 1]$): solve for $\underline{\varphi_0, f \text{ and } \varphi_1}$:

$$
\boxed{
\begin{aligned}
x'(s) &= \cos(\varphi(s)) & x(0) &= x_0 & x(1) &= \xi(\alpha) \\
y'(s) &= \sin(\varphi(s)) & y(0) &= y_0 & y(1) &= \eta(\alpha) \\
\varphi'(s) &= \kappa(s) & \varphi(0) &= \varphi_0 & \varphi(1) &= \varphi_1 \\
\kappa'(s) &= f \cos(\varphi(s) - \alpha) & & & \kappa(1) &= 0
\end{aligned}
}
\tag{19}
$$

Phase B ($s \in (0, s_1]$): solve for $\underline{\varphi_0, f \text{ and } s_1}$:

$$
\boxed{
\begin{aligned}
x'(s) &= \cos(\varphi(s)) & x(0) &= x_0 & x(s_1) &= \xi(\alpha) \\
y'(s) &= \sin(\varphi(s)) & y(0) &= y_0 & y(s_1) &= \eta(\alpha) \\
\varphi'(s) &= \kappa(s) & \varphi(0) &= \varphi_0 & \varphi(s_1) &= \alpha \\
\kappa'(s) &= f \cos(\varphi(s) - \alpha) & & & \kappa(s_1) &= 0
\end{aligned}
}
\tag{20}
$$

Once all parameters are known, they can be used to construct the elastic line of the vibrissa as well as the unknown support reactions:

holding moment: $m_0 = -m_{bz}(s \to 0) = -f((y_0 - \eta(\alpha))\sin(\alpha) + (x_0 - \xi(\alpha))\cos(\alpha))$

reaction forces: $f_{Ax} = -f\sin(\alpha), f_{Ay} = f\cos(\alpha)$.

First we simulate a single rotational sweep along a parabolic object contour function:

Profile I:

$$g_1 : x \longmapsto g_1(x) = 0.7x^2 + q \tag{21}$$

and investigate the observables (m_0, f_{Ax}, and f_{Ay}). The object distance parameter q is varied to clarify its influence on the scanning process.

The observables in Figure 3 do **not** enable a direct inference to the scanned profile contour. The transitions between Phases A and B are marked with an "o" (compare Step 2). Obviously, the scanning range is limited to an area with $\alpha > 0$, which is tantamount to the right side of the convex object. To enlarge the scanning range, we extend the scanning process with a view to the animal kingdom. Mice and rats sweep their vibrissae back and forth along objects during active whisking. To examine the benefit of this behavior we consider two rotational movements of the vibrissa from now on – one in a mathematical positive sense and an additional one in a negative sense. Furthermore, in order to demonstrate the general functionality of our scanning algorithm, we consider three different object contour functions:

Profile II: a parabola is

$$g_2 : x \longmapsto g_2(x) = 0.5x^2 + q. \tag{22}$$

Profile III: a semicircle (radius $r = 1$) is

$$g_3 : x \longmapsto g_3(x) = 1 - \sqrt{1 - x^2} + q. \tag{23}$$

Profile IV: a sectionally defined function is

$$g_4 : x \longmapsto g_4(x) = \begin{cases} 0.5x^2 + q & (-1 \le x < 0) \\ x^4 + q & (0 \le x \le 1). \end{cases} \tag{24}$$

Comparing Figures 4, 5, and 6 with Figure 3, it becomes clear that the scanning range is enlarged significantly by extending the scanning process. This provides us with new information about the symmetry of the object: The axial symmetry of Profiles II and III reappears in the observables (see Figures 4 and 5). The graphs of m_0 and f_{Ax} are point symmetric, because m_0 and f_{Ax} are exactly opposed during the backward scanning movement. The curve for f_{Ay} is axial symmetric because the reaction force must be positive for both directions of rotation. In contrast, the observables in Figure 6 show the asymmetry of Profile IV. Here, all observables contain qualitative disparities comparing the backward and forward movement.

All simulations demonstrate that it is possible to control the signal strength varying the object distance q. Thus, the signals at the support could be adapted for the measuring range of any sensor. It should be noted that for each simulation the curves of the observables have a gap in an area of $\alpha = 0$. This results from the abort of the scanning algorithm in the respective scanning direction.

To sum up, the extended scanning process enlarges the scanning range, which allows a first evaluation of the object symmetry. However, this is certainly not enough to be able to make an exact statement about the object contour. Thus, in a next step, we focus on reconstructing the object contour, using only the generated observables and the boundary conditions at the support of the rod.

4. Step 2, Reconstructing the Object Contour

Whereas until now we generated the observables solving the boundary-value problems (19) and (20), we now use these
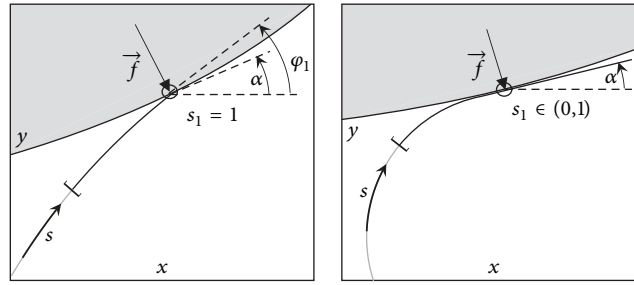
Figure 2: Comparison between contact Phases A (tip contact) and B (tangential contact).
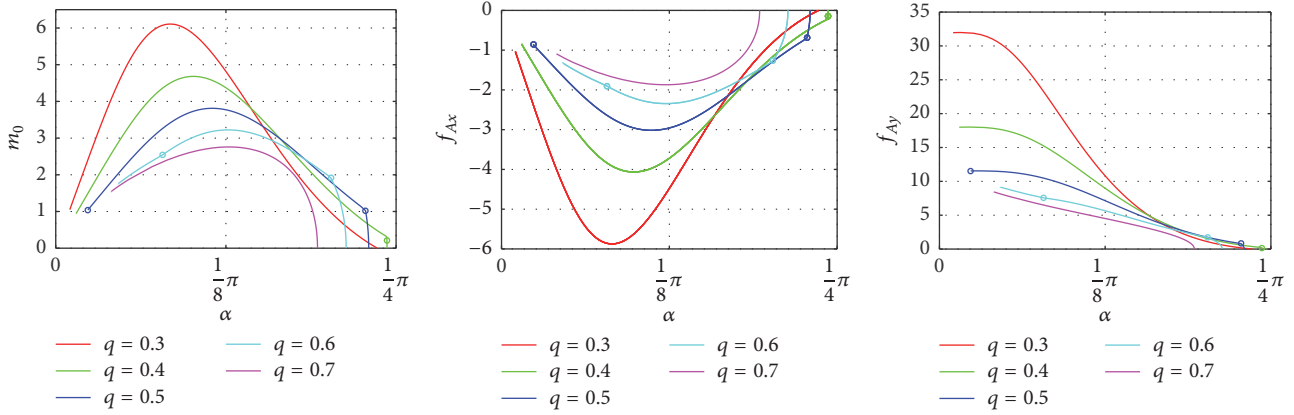

$q = 0.3$
$q = 0.4$
$q = 0.5$
$q = 0.6$
$q = 0.7$

Figure 3: Observables m_0, f_{Ax}, and f_{Ay} during a single scanning sweep along the parabolic Profile I.

$q = 0.3$
$q = 0.4$
$q = 0.5$
$q = 0.6$
$q = 0.7$
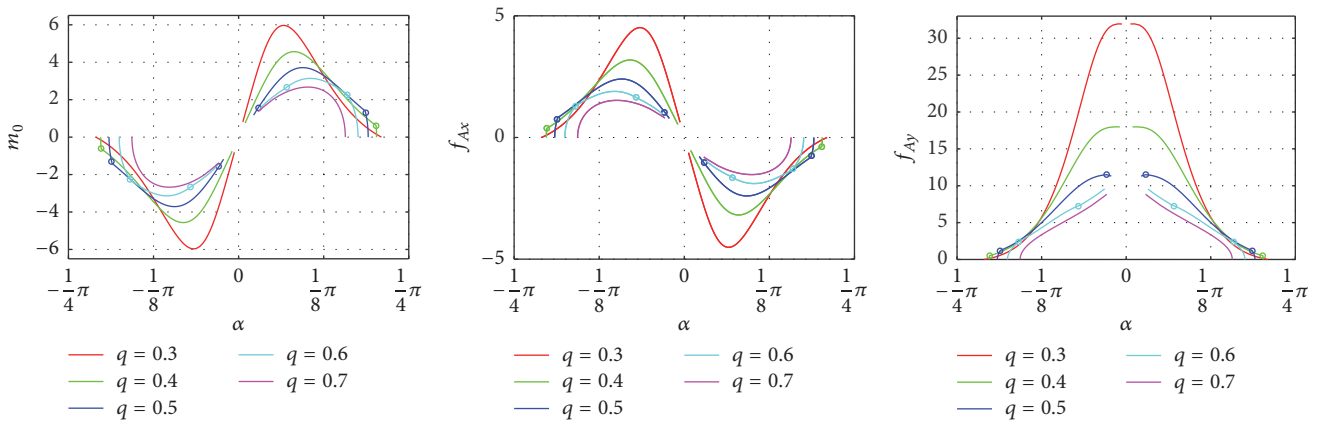
Figure 4: Observables m_0, f_{Ax}, and f_{Ay} during a forward and backward sweep along the parabolic Profile II.

$q = 0.3$
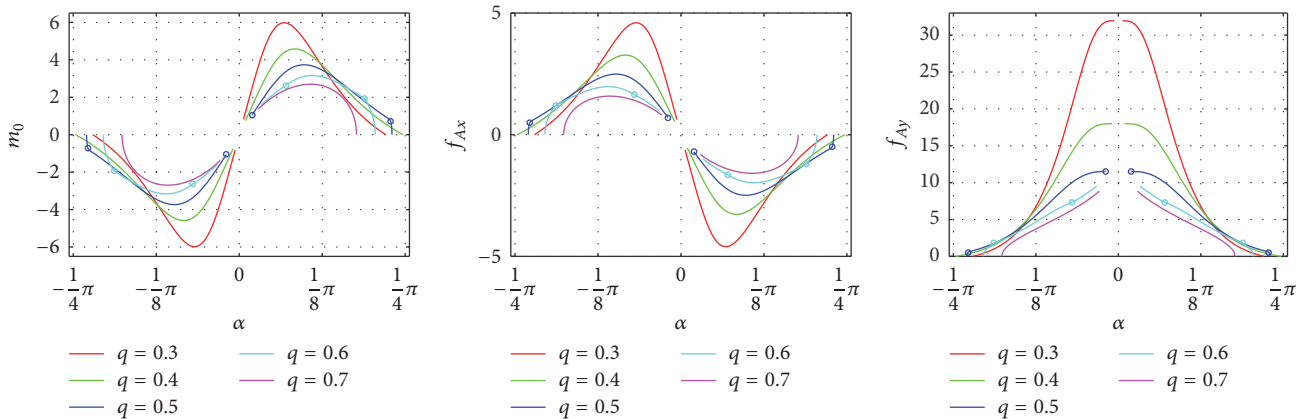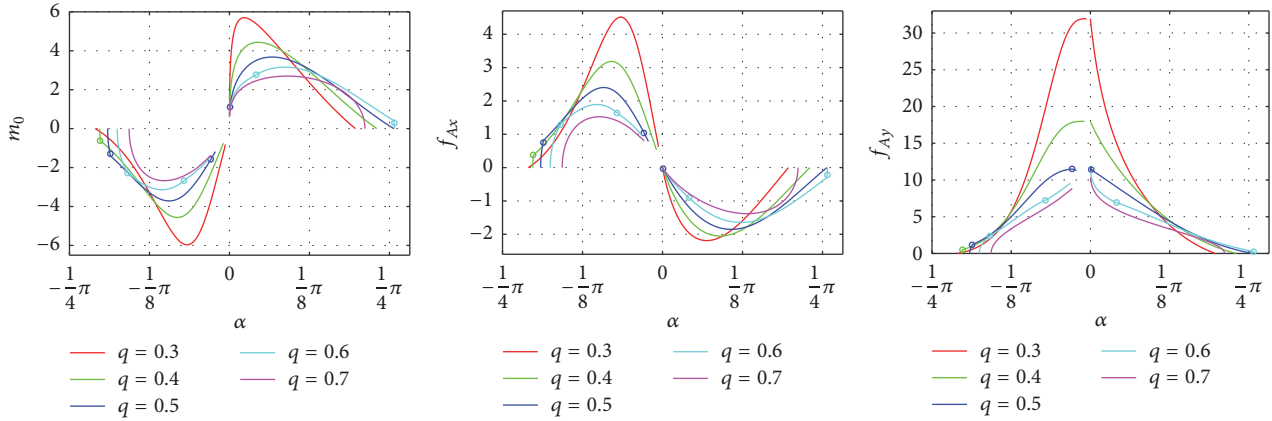$q = 0.4$
$q = 0.5$
$q = 0.6$
$q = 0.7$

Figure 5: Observables m_0, f_{Ax}, and f_{Ay} during a forward and backward sweep along the circular Profile III.

FIGURE 6: Observables m_0, f_{Ax}, and f_{Ay} during a forward and backward sweep along the asymmetric Profile IV.

quantities to reconstruct a sequence of contact points. Let the following quantities be given from the generation step (or an experiment):

$$f_{Ax}, f_{Ay}, m_0, x_0, y_0, \varphi_0 \tag{25}$$

In Step 2, the parameters f and α in (10d) are unknown but can easily be specified as a function of the known support reactions:

$$
\begin{aligned}
f &= \sqrt{f_{Ax}^2 + f_{Ax}^2}, \\
\alpha &= -\arctan\left(\frac{f_{Ax}}{f_{Ay}}\right)
\end{aligned}
\tag{26}
$$

For determining the contact position s_1 and so the contact point ($\xi(\alpha) = x(s_1)$, $\eta(\alpha) = y(s_1)$) we have to solve the initial-value problem (27) numerically with the abort criterion $\kappa(s_1) = 0$.

$$
\begin{array}{ll}
x'(s) = \cos(\varphi(s)) & x(0) = x_0 \\
y'(s) = \sin(\varphi(s)) & y(0) = y_0 \\
\varphi'(s) = \kappa(s) & \varphi(0) = \varphi_0 \\
\kappa'(s) = f\cos(\varphi(s) - \alpha) & \kappa(0) = -m_0
\end{array}
\tag{27}
$$

Once s_1 is known, we can construct the elastic line of the bending rod, when it is swept along an object, and reconstruct a sequence of contact points, which finally approximates the object contour.

Again, we consider the profiles I, II, III, and IV and construct the elastic line of the bending rod starting from the very first contact between the undeflected rod with the object (α_{Start}) and ending with the last equilibrium state (α_{Ende}) that can be found by the simulation algorithm. Tip contacts are colored in blue, tangential contacts are in red, and the transitions between the contact phases are black colored (compare with the phase transitions in Figures 3, 4, 5, and 6).

Looking at Figures 7, 8, 9, and 10 it becomes clear that the larger the object distance is, the more the tip contacts

occur, whereas tangential contacts increasingly occur with a decreasing object distance. The scanned area is limited by the profile parameters α_{Start} and α_{Ende}. For each scanning sweep the last elastic line (contact at α_{Ende}) is the last equilibrium state that can be computed by the algorithm.

Remark 4. Actually, it can be imagined that even in reality there would not be an equilibrium state anymore after exceeding a critical drive angle φ_0. Setting a higher drive angle, the vibrissa would just snap off of the object. Thus, the abort of the simulation algorithm might point out an exceedance of this critical snap off configuration.

Figure 11 shows the reconstructed sequences of contact points overlaid with each corresponding profile function. It becomes clear that contour reconstruction works well for all (symmetric and asymmetric) profiles and for all chosen object distances q.

Nevertheless, all reconstructed contours are severed by a small gap, resulting from the snap off (see the lack of observables in this area in Figures 3, 4, 5, and 6). It can be observed that the sizes of these reconstruction gaps increase for high object distances q, especially when the scanning sweep ends with a tip contact. In none of the cases do the scanning ranges of the forward and backward movement overlap, so we have to put up with the reconstruction gaps, when using only the rotatory scanning movement.

5. Conclusion and Outlook

In this paper, we presented a biologically inspired mechanical model for tactile shape recognition. In contrast to many previous publications, we adapted our model for a rotational scanning movement, which better matches animal's behavior during active whisking. The model consists of a single vibrissa, considered as a cylindrically shaped Euler-Bernoulli bending rod, which is pivoted by a bearing. Using nonlinear Euler-Bernoulli theory we derived a boundary-value problem with some unknown parameters, describing the elastic line of the rod, when it is deflected due to an object contact.
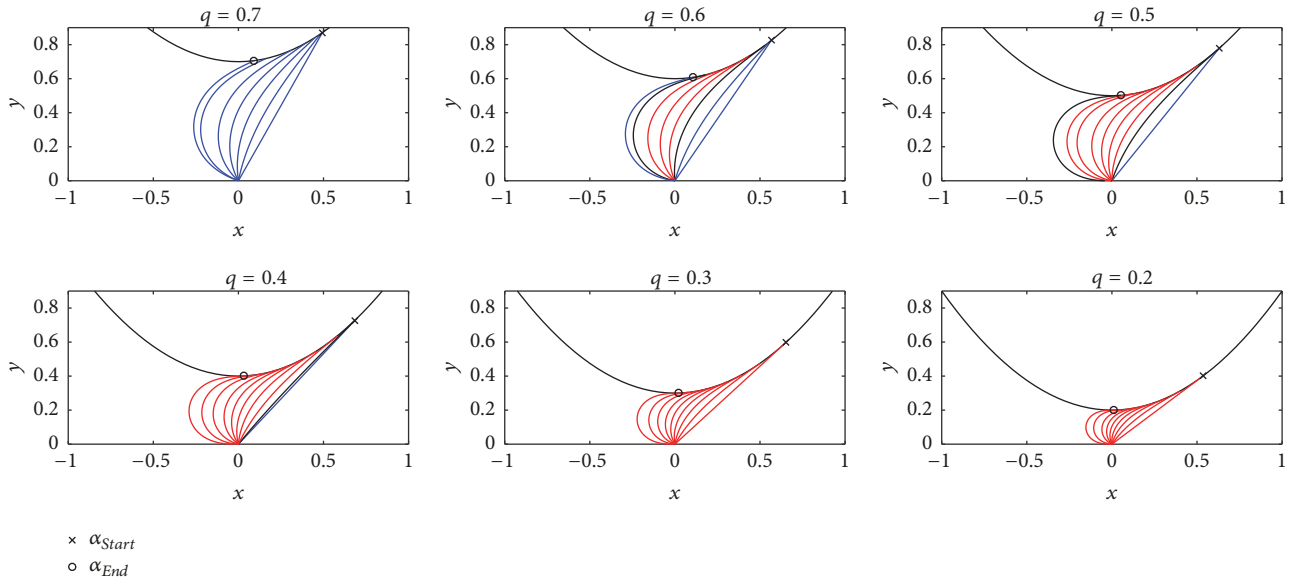
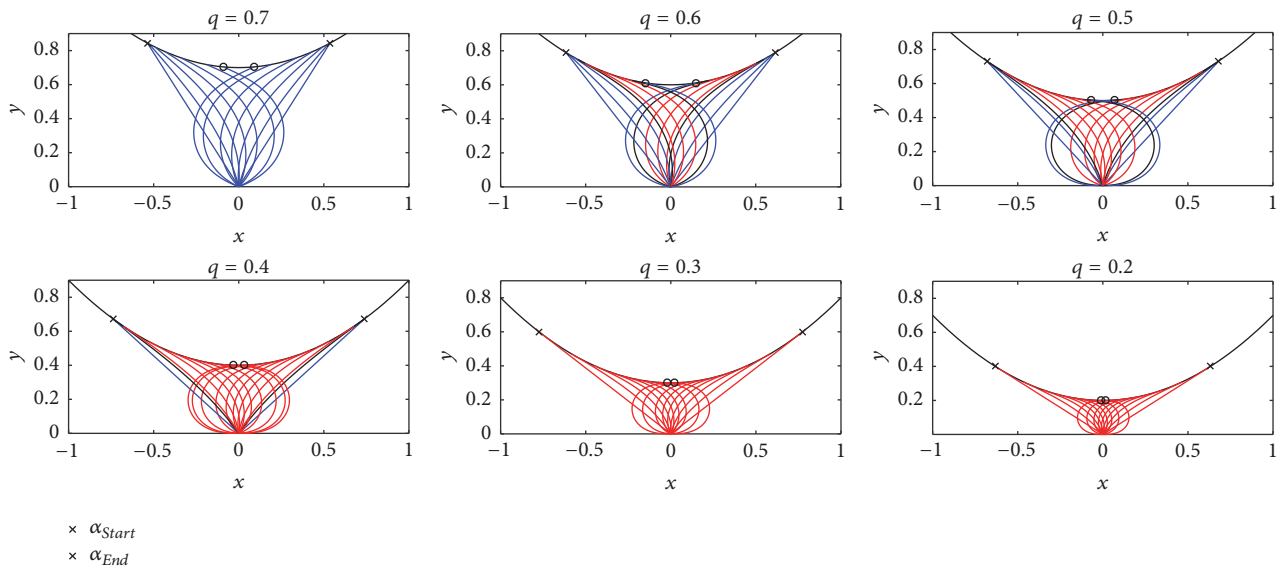FIGURE 7: Deformation states during a single sweep along Profile I.

FIGURE 8: Deformation states during a forward and backward sweep along Profile II.

Thus, instead of only relying on measured support reactions [18, 19], in a first step we used shooting methods in an algorithm in order to generate the support reactions (reaction forces and holding moment) during rotatory scanning any strict convex object profile. The ability of generating the observables during rotatory scanning is a major advantage compared to previous works, since it is a small step to adapt our algorithm in order to take more morphologic properties of the biological paradigm into account (e.g., the tapered and precurved shape of a vibrissa). Thus, the presented algorithm might be used in preliminary investigations to carry out parameter studies without the necessity of performing a large

number of experiments and without the need of several artificial vibrissae.

A first investigation of the simulation results showed the need of enlarging the scanning area. An approach to solve this problem was adopted from the biological paradigm: we enlarged the scanning procedure by an additional scanning sweep in opposite direction. We extended our investigations on four different object profiles to show the general applicability of our algorithm for strict convex contours. In all cases it was shown that the signal strength of the observables could be adapted for the measuring range of any sensor by changing the object distance. Contour information about the object
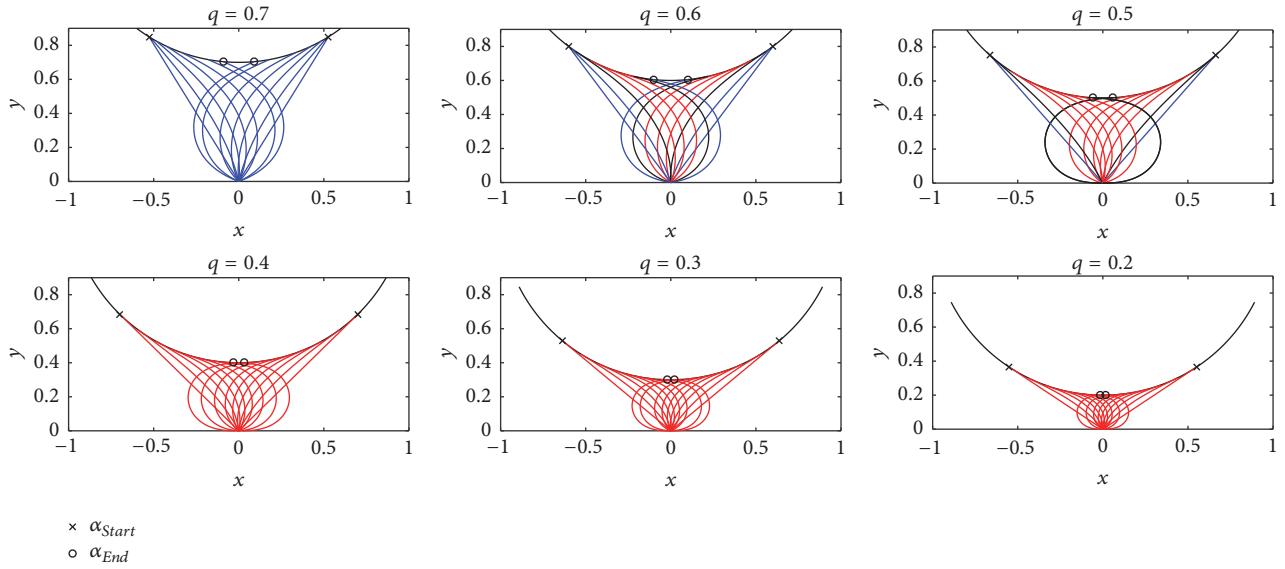
FIGURE 9: Deformation states during a forward and backward sweep along Profile III.
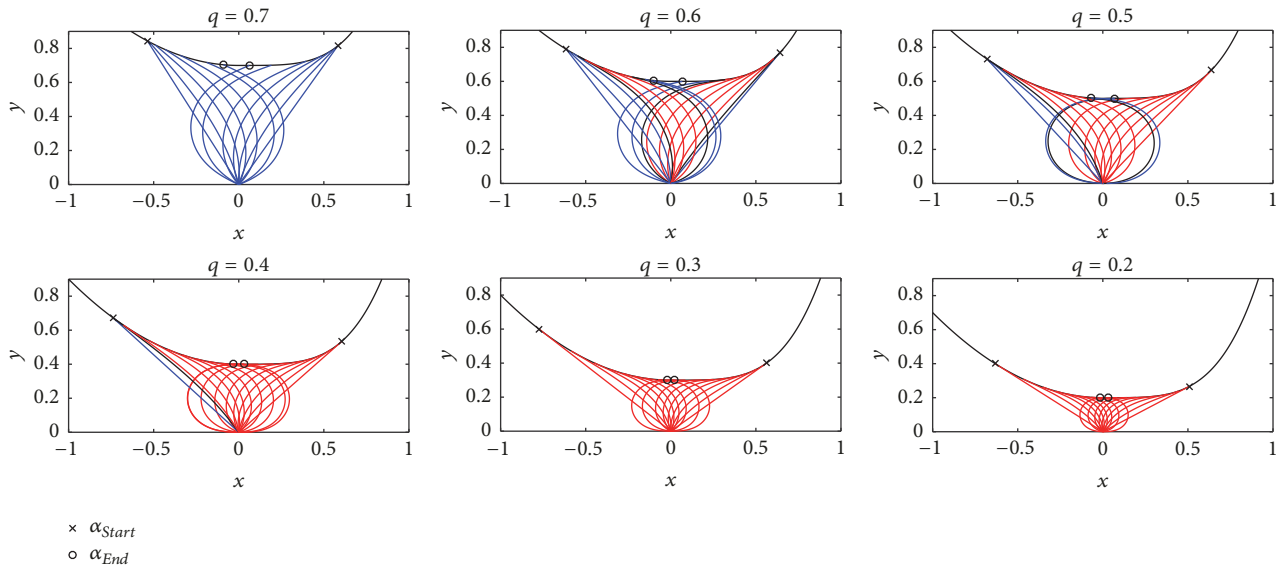

FIGURE 10: Deformation states during a forward and backward sweep along Profile IV.

was not too obvious looking at the observables so it required a further mathematical analysis: a reconstruction algorithm.

Then, it was shown that, knowing the observables together with the boundary conditions at the support, an initial-value problem has to be solved for reconstructing a contact point. Including this step (Step 2) in our algorithm, we were able to construct the elastic line of the bending rod during the scanning sweeps and to reconstruct a sequence of contact points for each of the previously considered profiles. This sequence of contact points approximates the object contour, as the simulations showed the scanning range was enlarged significantly by extending the scanning process.

In contrast to many previous publications like [11] or [12], where the support position has to be changed to scan a larger range of the object because small deflections are considered only, we showed that the reconstruction of a large part of the object worked well even for a single support position. Nevertheless, the present paper showed that the reconstructed areas of all profiles were severed by a small gap, which results from the bending rod snap off of the profile in both scanning directions.

Since this fact seems to be a general problem when using the rotational scanning procedure, a further enlargement of the scanning process could be a combined translational
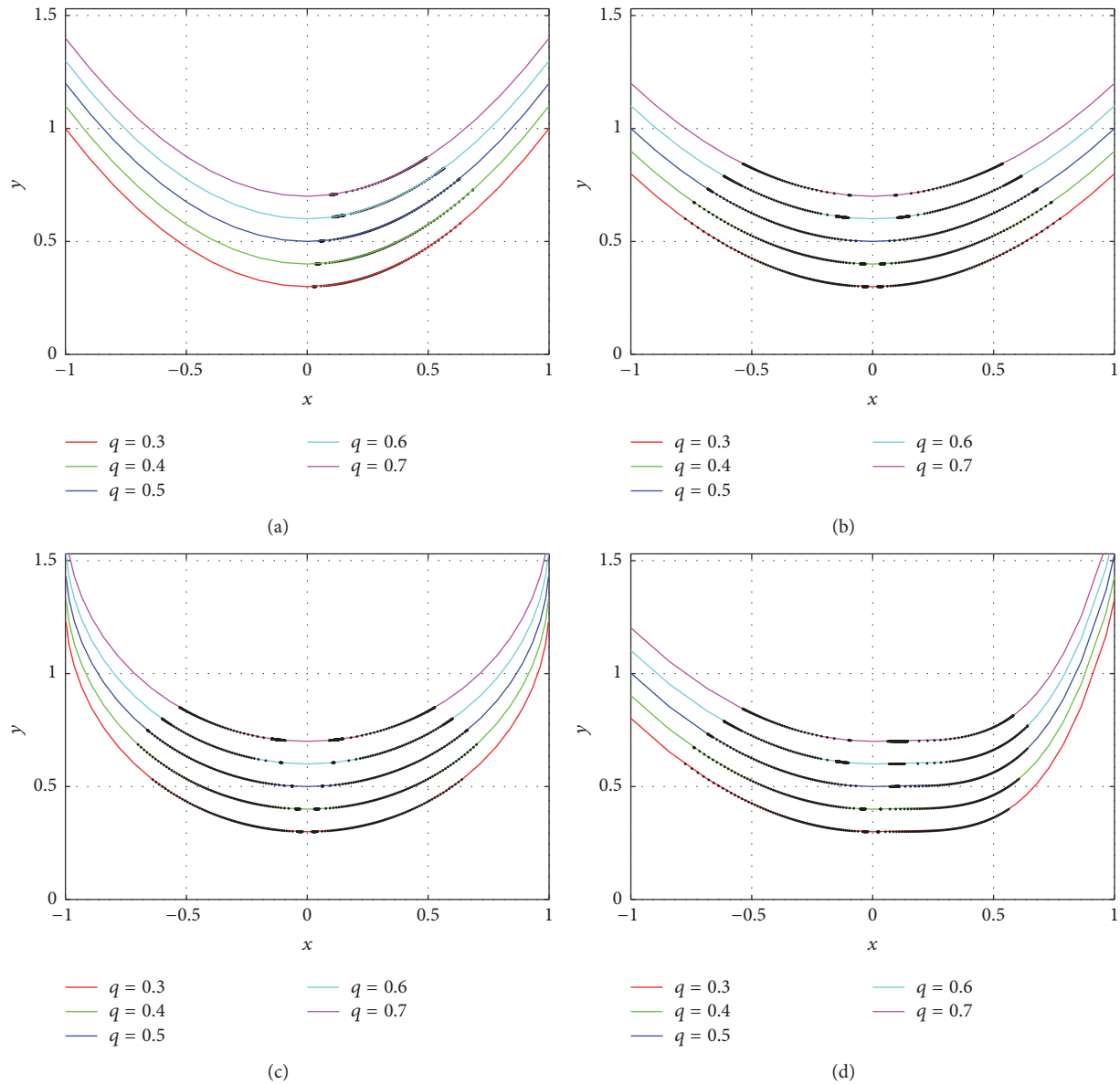
Figure 11: Reconstructed contact points overlaid with the scanned profile functions: (a) Profile I; (b) Profile II; (c) Profile III; (d) Profile IV.

and rotational movement. A largely analytical treatment of a translational scanning method can be found in [17]. In our case the following strategy would be conceivable: The support position could be shifted translationally in a horizontal direction after each rotational scan. Thus, a superimposition of a variety of rotational scans at different support positions would close the reconstruction gaps.

However, another way to close the scanning gaps could be to use a number of vibrissae with different support positions (vibrissae array) to avoid the necessity of shifting the support translationally. In addition another translational movement of the support could be allowed in a vertical direction in order to control the signal strength. All investigations conducted in this paper should be continued towards more involved models. Animal vibrissae actually are not cylindrically shaped as supposed here, but are tapered and precurved in certain ways [20–23].

Data Availability

The data used to support the findings of this study are available from the corresponding author upon request.

Conflicts of Interest

The authors declare that there are no conflicts of interest regarding the publication of this paper.

References

[1] S. Ebara, K. Kumamoto, T. Matsuura, J. E. Mazurkiewicz, and F. L. Rice, "Similarities and differences in the innervation of mystacial vibrissal follicle-sinus complexes in the rat and cat: A confocal microscopic study," *Journal of Comparative Neurology*, vol. 449, no. 2, pp. 103–119, 2002.

[2] J. Dörfl, "The musculature of the mystacial vibrissae of the white mouse," *Journal of Anatomy*, vol. 135, no. 1, pp. 147–154, 1982.

[3] B. Mitchinson, R. A. Grant, K. Arkley, V. Rankov, I. Perkon, and T. J. Prescott, "Active vibrissal sensing in rodents and marsupials," *Philosophical Transactions of the Royal Society B: Biological Sciences*, vol. 366, no. 1581, pp. 3037–3048, 2011.

[4] S. Hirose, S. Inoue, and K. Yoneda, "The whisker sensor and the transmission of multiple sensor signals," *Advanced Robotics*, vol. 4, no. 2, pp. 105–117, 1990.

[5] D. Jung and A. Zelinsky, "Whisker based mobile robot navigation," in *Proceedings of the 1996 IEEE/RSJ International Conference on Intelligent Robots and Systems, IROS. Part 3 (of 3)*, pp. 497–504, November 1996.

[6] D. Baldeweg, C. Will, and C. Behn, "Transversal vibrations of beams in context of vibrassae consisting of foundations, discrete supports and various sections," in *Proceedings of the in Proceedings 58th International Scientific Colloquium*, Ilmenau (Germany), 2014.

[7] M. Kaneko, N. Kanayama, and T. Tsuji, "Active antenna for contact sensing," *IEEE Transactions on Robotics and Automation*, vol. 14, no. 2, pp. 278–291, 1998.

[8] M. M. Svinin, M. Kaneko, and N. Ueno, "Active and passive strategies in dynamic contact point sensing by a flexible beam," in *Proceedings of the 1997 IEEE/RSJ International Conference on Intelligent Robot and Systems. Part 1 (of 3)*, pp. 84–90, September 1997.

[9] N. Ueno and M. Kaneko, "On a new contact sensing strategy for dynamic active antenna," in *Proceedings of the 1995 IEEE International Conference on Robotics and Automation. Part 1 (of 3)*, pp. 1120–1125, May 1995.

[10] J. A. Birdwell, J. H. Solomon, M. Thajchayapong et al., "Biomechanical models for radial distance determination by the rat vibrissal system," *Journal of Neurophysiology*, vol. 98, no. 4, pp. 2439–2455, 2007.

[11] D. Kim and R. Möller, "Biomimetic whiskers for shape recognition," *Robotics and Autonomous Systems*, vol. 55, no. 3, pp. 229–243, 2007.

[12] J. H. Solomon and M. J. Z. Hartmann, "Artificial whiskers suitable for array implementation: Accounting for lateral slip and surface friction," *IEEE Transactions on Robotics*, vol. 24, no. 5, pp. 1157–1167, 2008.

[13] J. Steigenberger, "A continuum model of passive vibrissae," Tech. Rep., Institute of Mathematics, Technische Universität Ilmenau, Germany, 2013.

[14] J. Steigenberger, C. Behn, and C. Will, "Mathematical model of vibrissae for surface texture detection," Tech. Rep., Institute of Mathematics, Technische Universität Ilmenau, Germany, 2015.

[15] C. Will, J. Steigenberger, and C. Behn, "Object contour reconstruction using bio-inspired sensors," in *Proceedings of the 11th International Conference on Informatics in Control, Automation and Robotics, ICINCO 2014*, pp. 459–467, aut, September 2014.

[16] C. Will, J. Steigenberger, and C. Behn, "Bio-inspired Technical Vibrissae for Quasi-static Profile Scanning," in *Informatics in Control, Automation and Robotics*, vol. 370 of *Lecture Notes in Electrical Engineering*, pp. 277–295, Springer International Publishing, Cham, 2016.

[17] C. Will, C. Behn, and J. Steigenberger, "Object contour scanning using elastically supported technical vibrissae," *ZAMM - Journal of Applied Mathematics and Mechanics*, vol. 98, no. 2, pp. 289–305, 2018.

[18] T. N. Clements and C. D. Rahn, "Three-dimensional contact imaging with an actuated whisker," *IEEE Transactions on Robotics*, vol. 22, no. 4, pp. 844–848, 2006.

[19] G. R. Scholz and C. D. Rahn, "Profile sensing with an actuated whisker," *IEEE Transactions on Robotics and Automation*, vol. 20, no. 1, pp. 124–127, 2004.

[20] C. Behn, J. Steigenberger, A. Sauter, and C. Will, "Pre-curved Beams as Technical Tactile Sensors for Object Shape Recognition," in *Proceedings of the The Fifth International Conference on Intelligent Systems and Applications (includes InManEnt)*, p. 12, 2016.

[21] S. A. Hires, L. Pammer, K. Svoboda, and D. Golomb, "Tapered whiskers are required for active tactile sensation," *eLife*, vol. 2013, no. 2, Article ID e01350, 2013.

[22] L. Pammer, D. H. O'Connor, S. A. Hires et al., "The mechanical variables underlying object localization along the axis of the whisker," *The Journal of Neuroscience*, vol. 33, no. 16, pp. 6726–6741, 2013.

[23] B. W. Quist and M. J. Z. Hartmann, "Mechanical signals at the base of a rat vibrissa: The effect of intrinsic vibrissa curvature and implications for tactile exploration," *Journal of Neurophysiology*, vol. 107, no. 9, pp. 2298–2312, 2012.

[24] L. Merker, C. Will, J. Steigenberger, and C. Behn, "Object contour sensing using artificial rotatable vibrissae," in Engineering for a Changing World: 59th IWK, Ilmenau Scientific Colloquium, Technische Universität Ilmenau, Germany, 2017.

[25] L. Euler, *Methodus inveniendi lineas curvas maximi minimive proprietate gaudentes, sive solutio problematis isoperimetrici latissimo sensu accepti*, Bousquet, Lausannæ, Genevæ, 1744.